Structural, spectral and magnetic properties of Ni(II), Co(II) and Cd(II) compounds with imidazole derivatives and silanethiolate ligands

D. Kowalkowska, A. Dołęga, N. Nedelko, Z. Hnatejko, Ł. Ponikiewski, A. Matracka, A. Ślawska-Waniewska, A. Strągowska, K. Słowy, M. Gazda and A. Pladzyk

A series of new metal heteroleptic complexes have been obtained in simple reactions of 1-(3-aminopropyl)-imidazole (api) and 1,4-bis(imidazol-1-yl)-butane (bbi) ligands with metal silanethiolates or acetylacetonates. The obtained complexes are the coordination polymers $[Ni\{SSi(tBuO)_3\}_2(\mu\text{-api})]_n$ **1**, $[Co\{SSi(tBuO)_3\}_2(\mu\text{-api})]_n$ **2**, $[Cd\{SSi(tBuO)_3\}_2(\mu\text{-api})\cdot 2CH_3OH]_n$ **3**, $[Cd\{SSi(tBuO)_3\}_2(\mu\text{-bbi})\cdot CHCl_3]_n$ **4** and the dimer $[Co\{SSi(tBuO)_3\}_2(\mu\text{-bbi})\cdot 3CH_3OH]_2$ **5**. Another coordination polymer with the formula $[Ni(acac)_2(\mu\text{-bbi})\cdot 9CHCl_3]_n$ **6** was obtained in the reaction of $Ni(acac)_2$ with $(tBuO)_3SiSH$ (TBST) and bbi; however, the silanethiolate residue didn't coordinate to the metallic center as intended. The molecular structures of **1–6** were determined by single-crystal X-ray diffraction. Compounds **1–5** were additionally characterized by thermogravimetry (TGA) and powder X-ray diffraction. The emission spectra of the Cd complexes **3** and **4** were recorded in the solid state at ambient temperature, whereas **1**, **2** and **5** were subjected to magnetic studies. Variable-temperature magnetic measurements of the polycrystalline sample **1** suggest the presence of weak intra-chain magnetic interactions between the nickel(II) ions. Magnetic studies of **2** and **5** show their paramagnetic behavior. For sample **1** as well as samples **2** and **5**, a noticeable influence of single-ion magnetic anisotropy on their magnetic behavior has been revealed.

DOI: 10.1039/c7ce00555e

Introduction

Imidazoles and thiolate residues have been shown to be multifunctional agents with significant meaning to life and science.[1] They are present in many biological systems[2,3] but also exhibit important pharmaceutical properties.[4–8] Further, they find use as model compounds for the design and synthesis of functional supramolecular constructs and are of interest as synthetic biomimetic compounds used in model studies of biological processes based on charge transfer mechanisms.[9–19]

Among the huge mass of compounds containing thiolates and imidazoles as N,S-donor set heteroligands, there are only some examples where metal ions are coordinated by RS^- and imidazoles as discrete ligands.[20–22] Reactions of thiols with metal ions often lead to non-defined polymers. Our previous research has proven that the use of organoxysilanethiols with bulky substituents on the silicon atom allows the bypassing of this inconvenience. Among them tri-*tert*-butoxysilanethiol $(tBuO)_3SiSH$ (TBST) turned out to be fairly stable under atmospheric conditions.[23] Another organoxysilanethiol relatively resistant towards hydrolysis – tris(2,6-diisopropylphenoxy)-silanethiol (TDST) – was obtained quite recently and its coordination properties are still under examination.[24] Both silanethiols contain bulky alkoxy/aryloxy substituents on the silicon atom which effectively inhibit the tendency of thiols to form polymeric complexes and enable the obtainment of numerous neutral and ionic mono- and polymetallic complexes by coordination as an S-monodentate, an S,O-bidentate and S-bridging ligands.[25] Among the silanethiolate complexes are those which contain metals additionally coordinated by flexible aliphatic diamines,[26] as well as rigid pyridine[27] and imidazole derivatives;[28] some of the obtained compounds exhibit interesting luminescence and magnetic properties.

As a continuation of our studies carried out previously and to fully explore the relations between the type of ligand and properties of obtained metal silanethiolates, we decided

[a] *Department of Inorganic Chemistry, Chemical Faculty, Gdańsk University of Technology, Narutowicza Str. 11/12, 80-233 Gdańsk, Poland. E-mail: agnieszka.pladzyk@pg.edu.pl*
[b] *Institute of Physics, Polish Academy of Sciences, Aleja Lotników 32/46, 02-668 Warsaw, Poland*
[c] *Department of Rare Earths, Faculty of Chemistry, Adam Mickiewicz University, Umultowska 89b, 61-414 Poznań, Poland*
[d] *Department of Solid State Physics, Faculty of Applied Physics and Mathematics, Gdańsk University of Technology, Narutowicza Str. 11/12, 80-233 Gdańsk, Poland*

to use spacers containing both flexible and rigid fragments in their structures. For this purpose, we choose 1-(3-aminopropyl)-imidazole (api) and 1,4-bis(imidazol-1-yl)-butane (bbi), which additionally can act as either N-monodentate and N,N-bidentate chelating or bridging ligands (Fig. 1). Herein, we describe the syntheses, crystal structures, and spectral and magnetic properties of six new Ni(II), Co(II) and Cd(II) coordination complexes with api, bbi, acac and $(t\mathrm{BuO})_3\mathrm{SiS}^-$ ligands and among them we describe the first tetrahedral Ni silanethiolate (Fig. 2). So far, to the best of the knowledge of the authors, no metal thiolates with api and bbi ligands coordinated to the metallic center have been reported.

Experimental

Materials and methods

Tri-*tert*-butoxysilanethiol $(t\mathrm{BuO})_3\mathrm{SiSH}$ (TBST), $[\mathrm{Co}\{\mathrm{SSi}(t\mathrm{BuO})_3\}_2(\mathrm{NH}_3)]_2$ and $[\mathrm{Cd}\{\mathrm{SSi}(t\mathrm{BuO})_3\}_2]_2$ were synthesized as reported previously.[23,29,30] 1,4-bis(imidazol-1-yl)-butane (bbi) was synthesized according to a reported procedure[31] with some modifications (Fig. S1 and experimental part in the ESI†). All other materials were obtained from commercial sources without further purification.

The elemental analyses (C, H, S and N contents) were performed using an Elemental Analyser EA 1108 (Carlo Erba Instruments). Thermogravimetric analysis was performed by using a Netzsch thermobalance TG 209 coupled with a Bruker IFS66 FTIR spectrometer under an atmosphere of argon. The volatiles evolving from the heated sample were transported to the spectrometer chamber through a thermostated pipe in the stream of argon.

The IR spectra were measured for crystalline compounds in the range of 4000 to 400 cm^{-1} with a Nicolet iS50 FTIR spectrometer equipped with the Specac Quest single-reflection diamond attenuated total reflectance (ATR) accessory. Spectral analysis was controlled by the OMNIC software package. The electronic absorption spectra of the ligands api and bbi and complexes **3** and **4** were recorded with a Shimadzu UVPC 2001 spectrophotometer. Magnetic measurements were carried out on polycrystalline samples using a commercial Physical Property Measurement System (PPMS, Quantum Design). The magnetization (M) was measured in the temperature range 2–300 K upon heating under a dc magnetic field (H = 1 kOe) in both zero-field-cooling (ZFC) and field-cooling (FC) regimes. The isothermal magnetization curves were measured in the magnetic field range ±9 T at selected temperatures in the 2–300 K range. The dynamic properties were studied with an ac susceptometer in zero external dc field at an exciting field of 3 Oe at selected frequencies in the range 10 Hz–10 kHz. Data were corrected for the sample-holder contribution and diamagnetism of the sample using standard procedures.[32,33] The single crystal X-ray diffraction data of compounds **1**–**3** and **5** were collected using a Stoe IPDS-2 T diffractometer with graphite-monochromated Mo-Kα radiation; crystals were cooled using a Cryostream 800 open flow nitrogen cryostat (Oxford Cryosystems). Data collection and image processing was performed with X-Area 1.75.[34] Intensity data were scaled with LANA (part of X-Area) in order to minimize differences of intensities of symmetry-equivalent reflections (multi-scan method). The diffraction data of **4** were collected using a diffractometer equipped with a Bruker image plate detector system IPDS using CuK_α radiation with graphite monochromatization (λ = 0.71073 Å). The experimental diffraction data of **6** were collected using a KM4CCD kappa-geometry diffractometer equipped with a Sapphire2 CCD detector. An enhanced X-ray Mo K_α radiation source with a graphite monochromator was used. The data were processed using the CrysAlisPro (Oxford Diffraction) program package.[35] Good quality single-crystal specimens of **4** and **6** were selected for the X-ray diffraction experiments at 293 K. The structures of **1**–**6** were solved by direct methods and all non-hydrogen atoms were refined with anisotropic thermal parameters by a full-matrix least squares procedure based on F^2 using the SHELX–2014 program package.[36] The Wingx[37] and Olex[38] program suites were used to prepare the final versions of cif files. Hydrogen atoms were usually refined using an isotropic

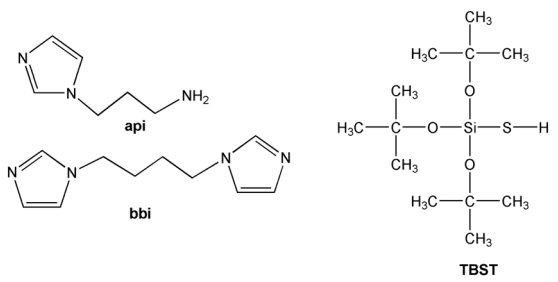

Fig. 1 Ligand structures.

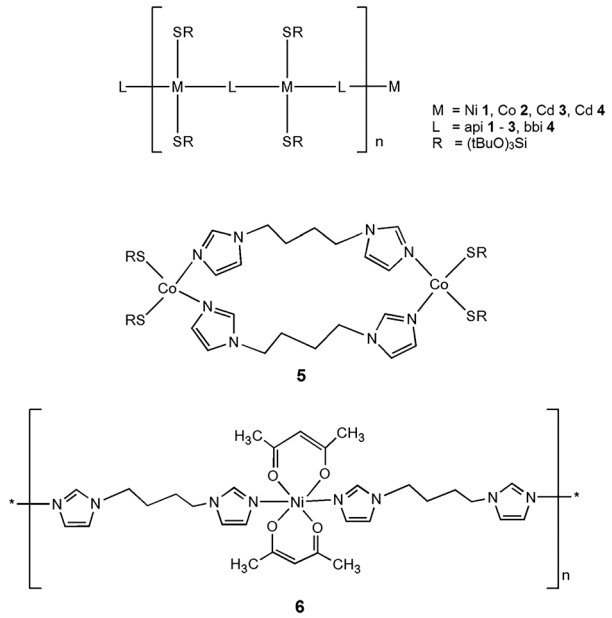

Fig. 2 Obtained complexes **1**–**6**.

model with $U_{iso}(H)$ values fixed to be 1.5 times U_{eq} of C atoms for $-CH_3$ or 1.2 times U_{eq} for $-CH_2$ and –CH groups. Disordered molecules of methanol present in the crystals of compounds **1** and **2** were removed from the final solution using the program PLATON, function SQUEEZE.[39]

The crystal parameters and refinement details are summarized in Table 1. The crystallographic data (without structure factors) for the structures reported in this paper have been deposited with the Cambridge Crystallographic Data Centre with reference number CCDC 1538062 (**1**), 1538061 (**2**), 1538063 (**3**), 1538067 (**4**), 1538068 (**5**) and 1538070 (**6**). Powder X-ray diffraction patterns (XRD) were recorded by using an X'Pert Pro diffractometer with Cu K_α radiation. The scans were collected in the 2θ range of 5 to 50.

Synthesis

$[Ni\{SSi(tBuO)_3\}_2(\mu\text{-api})]_n$ 1. $NiCl_2{\cdot}6H_2O$ (0.119 g, 0.5 mmol) was dissolved in 50 mL of distilled water, and 25% solution of ammonia (0.149 mL, 2 mmol) was added followed by 1-(aminopropyl)-imidazole (0.239 mL, 2 mmol) and tri-*tert*-butoxysilanethiol (0.303 mL, 1 mmol). The reaction flask was closed with a rubber septum and vigorously shaken for *ca.* 1 hour. The obtained blue precipitate was filtered and recrystallized from methanol. The mixture was left at room temperature and after a week blue crystals were obtained. Yield: 87%. The compound decomposes at 185–187 °C. Anal. calc. for $C_{30}H_{65}N_3O_6S_2Si_2Ni$ (742.85): C, 48.51; H, 8.82; N, 5.66; S, 8.63%. Found: C, 47.42; H, 8.66; N, 5.66; S, 8.22%. IR (solid state) ν [cm^{-1}] = 3273 (w, br), 3162 (w), 3114 (w, br), 2971 (vs, sh), 2929 (s, sh), 2872 (m), 1590 (w, br), 1528 (w), 1471 (w), 1387 (m, sh) 1362 (s, sh), 1238 (s, sh), 1186 (s), 1116 (w, sh), 1098 (w, sh), 1040 (vs), 1018 (vs), 992 (vs), 908 (w), 822 (m, sh), 803 (m, sh), 755 (w), 687 (m), 647 (m), 545 (m, sh), 483 (w), 459 (w), 424 (w).

$[Co\{SSi(tBuO)_3\}_2(\mu\text{-api})]_n$ 2. $[Co\{SSi(tBuO)_3\}_2(NH_3)]_2$ (0.0634 g, 0.5×10^{-4} mmol) was dissolved in 20 ml of methanol, and 1-(3-aminopropyl)-imidazole was added (0.024 mL, 2×10^{-4} mmol). Compound **2** crystallizes rapidly, producing small blue crystals. Yield: 68%. Anal. calc. for $C_{30}H_{62}N_3O_6S_2Si_2Co$: C, 48.22; H, 8.62; N, 5.44; S, 8.30%. Found: C, 48.02; H, 8.70; N, 5.65; S, 8.10%. D.p. 198–199 °C. IR (solid state) ν [cm^{-1}] = 3332 (w), 3292 (w), 3244 (w), 3113 (m), 2929 (s), 2969 (m, sh), 1590 (w), 1523 (d, m), 1471 (m), 1386 (s, sh), 1362 (s, sh), 1237 (s, sh), 1182 (s, sh), 1113 (m, sh), 1097 (m), 1039 (vs), 1019 (vs), 987 (vs), 908 (w), 819 (d, s), 756 (m), 684 (s), 650 (vs), 546 (s), 479 (m), 459 (m), 422 (m).

$[Cd\{SSi(tBuO)_3\}_2(\mu\text{-api}){\cdot}2CH_3OH]_n$ 3. A portion of 1-(aminopropyl)-imidazole (0.024 mL, 0.2 mmol) was added to $[Cd\{SSi(tBuO)_3\}_2]_2$ (0.134 g, 0.1 mmol) dissolved in methanol (25 mL). The obtained mixture was left to stand at room temperature. After several hours, colorless crystals of **3** were collected. Yield: 66%. M.p. 177–178 °C. Anal. calc. for $C_{62}H_{120}N_6O_{14}S_4Si_4Cd_2$ (1639.07): C 45.43; H, 7.38; N, 5.13; S, 7.83%. Found: C 45.05; H, 8.27; N, 5.29; S, 7.55%. IR (solid state) ν [cm^{-1}] = 3361 (w), 3299 (w), 3105 (w), 3092 (s, sh), 3028 (w), 2970 (vs, sh), 2927 (s, sh), 2867 (m), 1586 (w, br), 1514 (m), 1452 (m, br), 1385 (s), 1362 (s), 1244 (m, sh), 1185 (s, sh), 1180 (w), 1116 (w), 1097 (m), 1039 (vs, sh), 998 (vs), 957 (m), 937 (m), 909 (w), 823 (s), 818 (m), 800 (m), 774 (m), 688 (s), 651 (s), 545 (s), 510 (m), 495 (m), 479 (m), 420 (w).

$[Cd\{SSi(tBuO)_3\}_2(\mu\text{-bbi}){\cdot}CHCl_3]_n$ 4. $[Cd\{SSi(tBuO)_3\}_2]_2$ (0.134 g, 0.1 mmol) dissolved in chloroform (10 mL) was mixed with 1,4-bis(imidazol-1-yl)-butane (0.076 g,0.4 mmol) dissolved in 5 mL of chloroform. The mixture was left at 4 °C for crystallization and after one month colorless crystals of **4** were obtained. Yield: 48%. D.p. 151–155 °C. Anal. calc. for $C_{35}H_{69}Cl_3N_4O_6S_2Si_2Cd$ (981.02): C 42.85; H, 7.09; N, 5.71; S, 6.54%. Found: C 44.78; H, 7.48; N, 6.43; S, 6.68%. IR (solid state) ν [cm^{-1}] = 3413 (w, br), 3168 (w, br), 3112 (w, sh), 2972 (vs, sh), 2927 (s), 2867 (w), 1515 (m), 1470 (w), 1387 (m), 1363 (s), 1236 (m), 1184 (s), 1109 (w), 1093 (m), 1039 (vs, sh), 1014 (vs), 935 (m), 819 (s), 802 (s), 750 (m), 682 (s), 643 (s), 542 (m, sh), 500 (w), 475 (m), 419 (w).

$[Co\{SSi(tBuO)_3\}_2(\mu\text{-bbi}){\cdot}3CH_3OH]_2$ 5. $[Co\{SSi(tBuO)_3\}_2(NH_3)]_2$ (0.13 g, 0.1 mmol) was dissolved in 10 mL of methanol, and 1,4-bis(imidazol-1-yl)-butane (0.038 g, 0.12 mmol) dissolved in 5 mL methanol was added. Blue crystals of **5** were obtained after 24 h crystallization at room temperature. Yield: 65%. Anal. calc. for $C_{74}H_{160}N_8O_{18}S_4Si_4Co_2$ (1808.56): C, 49.14; H, 8.91; N, 6.19; S, 7.09%. Found: C, 49.77; H, 8.51; N, 6,17; S, 7.11%. D.p. 197–198.5 °C. IR (solid state) ν [cm^{-1}] = 3535 (s, br), 3115 (m), 2972 (vs), 2928 (m), 2869 (w), 2822 (w), 1574 (w), 1525 (s), 1468 (m), 1385 (s), 1365 (vs) 1287 (w), 1239 (s), 1188 (s), 1098 (m), 1011 (vs, br), 950 (m), 911 (w), 821 (m), 802 (m), 732 (w), 684 (s), 647 (s), 542 (s), 478 (w), 421 (w).

$[Ni(acac)_2(\mu\text{-bbi}){\cdot}9CHCl_3]_n$ 6. $Ni(acac)_2{\cdot}2H_2O$ (0.051 g, 0.2 mmol) dissolved in chloroform (10 mL) was mixed with 1,4-bis(imidazol-1-yl)-butane (0.076 g, 0.4 mmol) dissolved in 5 mL of chloroform. After one month, blue crystals of **6** were obtained. D.p. 215 °C Anal. calc. for $C_{40}H_{56}N_8O_8Ni_2$ (894.31): C 53.72; H, 6.31; N, 12.53%. Found: C 53.69; H, 6.29; N, 12.51%. IR (solid state) ν [cm^{-1}] = 3124 (w), 2986 (m), 2913 (w), 1648 (w), 1585 (vs), 1513 (vs), 1455 (vs), 1405 (vs), 1260 (w), 1253 (m), 1229 (m), 1194 (m), 1089 (d, m), 1010 (m), 920 (m), 826 (w), 731 (s), 660 (s), 625 (w), 565 (w), 411 (w).

Results and discussion

Complex syntheses and structures

Compound $[Ni\{SSi(tBuO)_3\}_2(\mu\text{-api})]_n$ **1** was obtained in a simple reaction of a nickel ammine complex prepared *in situ* from $NiCl_2$ in aqueous ammonia with $(tBuO)_3SiSH$ and api added in this order. The blue-violet precipitate was obtained almost immediately after adding api; nevertheless, the reaction mixture was further shaken for *ca.* 1 hour to allow all reagents to react completely. The obtained precipitate was filtered and then recrystallized from methanol resulting in blue crystals of **1**. This recrystallization was quite difficult because **1** was practically insoluble in the majority of solvents, showing a slight solubility in methanol which was finally used to obtain X-ray quality crystals. The X-ray analysis shows that **1**

Table 1 Crystallographic data and structure refinement results for **1–6**

Compound	**1**	**2**	**3**	**4**	**5**	**6**
Empirical formula	$C_{30}H_{65}N_3NiO_6S_2Si_2$	$C_{30}H_{62}N_3CoO_6S_2Si_2$	$C_{62}H_{120}N_6Cd_2O_{14}S_4Si_4$	$C_{35}H_{69}N_4CdCl_3O_6S_2Si_2$	$C_{74}H_{160}N_8Co_2O_{18}S_4Si_4$	$C_{49}H_{65}N_8Ni_2Cl_{27}O_8$
M_r/g mol^{-1}	742.86	740.05	1639.03	980.99	1808.55	1968.66
T (K)	120(2)	120(2)	120(2)	120(2)	120(2)	120(2)
Wavelength/Å	0.71073 (Mo K_α)	0.71073 (Mo K_α)	0.71073 (Mo K_α)	0.71073 (Mo K_α)	0.71073 (Mo K_α)	0.71073 (Mo K_α)
Crystal system	Monoclinic	Monoclinic	Monoclinic	Monoclinic	Triclinic	Triclinic
Space group	$P2_1/c$	$P2_1/a$	Pn	$P2_1/c$	$P\bar{1}$	$P\bar{1}$
a (Å)	14.3711(16)	9.592(3)	17.9772(18)	10.0110(3)	11.947(7)	14.0403(7)
b (Å)	11.9655(8)	33.010(8)	9.0260(10)	28.3797(13)	15.360(14)	16.2198(8)
c (Å)	9.5370(11)	14.296(4)	27.903(3)	18.2009(7)	15.374(17)	18.3694(9)
α (°)	90	90	90	90	90.85(8)	87.591(4)
β (°)	103.618(9)	103.94(2)	103.161(8)	99.872(3)	112.01(7)	78.654(4)
γ (°)	90	90	90	90	92.77(6)	88.153(4)
V (Å^3)	4389.3(10)	4393(2)	4408.7(8)	5094.5(3)	2611(4)	4096.7(4)
Z	4	4	2	4	1	2
Crystal size (mm)	0.25 × 0.07 × 0.6	0.04 × 0.15 × 0.38	0.22 × 0.28 × 0.38	0.21 × 0.22 × 0.23	0.131 × 0.18 × 0.242	0.21 × 0.22 × 0.24
D_{calc} (mg m^{-3})	1.124	1.119	1.235	1.279	1.15	1.596
θ range (°)	2.521 to 25.999	3.00 to 26.00	3.081 to 25.997	1.83 to 26.00	2.657 to 26.498	2.386 to 26.999
Reflections collected	33 287	21 322	98 888	36 057	20 390	27 311
Unique	8596	8488	16 638	9916	10 568	17 364
R_{int}	0.0759	0.0862	0.0586	0.064	0.0882	0.0737
μ (mm^{-1})	0.628	0.576	0.684	0.755	0.501	1.39
GOOF on F^2	1.061	0.955	1.048	0.92	0.913	1.056
R_1, wR_2 [$I > 2\sigma(I)$]	0.0518, 0.1492	0.0618, 0.1281	0.0388, 0.0783	0.0539, 0.126	0.0671, 0.1485	0.0867, 0.2129
R_1, wR_2 (all data)	0.0834, 0.2048	0.1354, 0.157	0.0375, 0.0799	0.0957, 0.1376	0.1406, 0.18	0.1368, 0.2788
$\Delta\rho_{max}$, $\Delta\rho_{max}$, e Å^{-3}	0.838, −0.885	1.248, −0.517	0.683, −0.455	1.415, −0.891	1.77, −1.148	3.072, −0.906
CCDC number	1538062	1538061	1538063	1538067	1538068	1 538 070

is polymeric with the formula $[Ni\{SSi(tBuO)_3\}_2(\mu\text{-api})]_n$ where Ni atoms are coordinated by two sulfur atoms from two terminal $(tBuO)_3SiS^-$ residues and two nitrogen atoms from two api ligands which link the neighboring Ni atoms (Fig. 1 and 3). The compound crystallizes in the $P2_1/c$ space group of the monoclinic system and the asymmetric unit consists of a Ni(II) ion, two terminal $(tBuO)_3SiS^-$ and one api ligand. Bond angles around Ni fall in the range 99.2(1)–131.32(4)° and point at a distorted tetrahedral geometry (τ_4 = 0.83).[40] The Ni(II) ion forms short Ni–N bonds (1.988(3) and 2.012(4) Å), with the shorter one formed with the imidazole ring. Ni–S bonds 2.290(1) and 2.265(1) Å are comparable with similar bonds in other tetrahedral nickel(II) silanethiolates (Table S1 in the ESI†).[41] The spatial arrangement of ligands makes the polymeric chain of **1** strongly folded, as shown in Fig. 3 and S2 in the ESI.† A closer look into the crystal structure reveals that there are intramolecular non-covalent interactions which with no doubt influence the final arrangement of the polymeric strings of **1**. The first type of hydrogen bonding interaction observed is N_{api}–H···$O_{silanethiolate}$ built by an ammine residue from api and two O atoms from *tert*-butoxyl residues and their length distances are almost identical (D···*A* 2.941(5) and 2.948(5) Å) (Table S3 in the ESI†). The second type of recognized interaction is C–H···$\pi_{imidazole}$ of bifurcated type formed between C–H of the carbonyl chain of api and two imidazole rings from the adjacent molecules of api. The C(30)–H(30)···π(centroid) distances are 3.564 Å within the same api ligand and 3.749 Å to the adjacent api. As a result, the closest Ni···Ni distance in the same chain is 7.504(1) Å and 12.621(2) Å between the neighboring chains. Api used in the reaction with $[Co\{SSi(tBuO)_3\}_2(NH_3)]_2$ also gave the coordination polymer $[Co\{SSi(tBuO)_3\}_2(\mu\text{-api})]_n$ **2** which is isostructural with **1**, and the overlay of the unit cells of **1** and **2** is shown in Fig. S3 (in the ESI†). The Co(II) atom displays a distorted tetrahedral coordination environment being coordinated by two S atoms of $(tBuO)_3SiS^-$ residues and two N atoms from two api molecules which link successive metallic centres. Co-based angles differ from the ideal tetrahedral geometry and vary from 102.9(2) to 119.55(5)° with the widest S–Co–S angle (τ_4 = 0.96) but these distortions are smaller than in **1** and they do not influence the Co–S and Co–N bond distances which are comparable with those in other tetrahedral Co(II) silanethiolates (Table S1 in the ESI†).[26,28,42] Intramolecular N_{api}–H···$O_{silanethiolate}$ (D···A 2.962 and 2.963 Å) and C–H···$\pi_{imidazole}$ (D···A 3.576 and 3.871 Å) interactions are also present in the structure of **2** and they force the arrangement of the chain which is strongly bent, just as in **1** (Fig. S4 in the ESI†). As a consequence, Co atoms are located at distances of 7.470(2) Å in the chain similar to that observed in **1** and 12.757(3) Å between the neighboring chains of **2**.

The coordination polymer $[Cd\{SSi(tBuO)_3\}_2(\mu\text{-api})\cdot 2CH_3OH]_n$ **3** was also obtained in the reaction of api with cadmium silanethiolate $[Cd\{SSi(tBuO)_3\}_2]_2$ (Fig. 4). The compound crystallizes in the *Pn* space group of the monoclinic system and contains four-coordinated Cd atoms which adopt a distorted tetrahedral geometry (τ_4 = 0.85) with angles ranging from 90.3(2) to 124.93(5)° and the narrowest N–Cd–N and the widest S–Cd–S among them (Table S1 in the ESI†).

The chains of **3** are less bent than in the previous polymers, and Cd atoms are separated by 9.229 Å within the same chain.

A deeper investigation of the crystal structure of **3** highlighted that the molecules of methanol are crucial for the crystal packing, because they are engaged in the formation of a net of diverse intermolecular hydrogen bond interactions, *i.e.* as a donor of $O_{methanol}$–H···$S_{silanethiolate}$ (D···A 3.179 Å) and as an acceptor of N_{api}–H···$O_{methanol}$ (D···A 2.954 Å) (Table S3 in the ESI†). Moreover, we think that weak C_{api}–H···$C_{methanol}$ interactions are also important for the spatial packing of **3** (D···A 3.569 Å) to a certain extent and together with the former interactions should be taken into account as these hold the whole structure together. Therefore, the spatial structure of **3** can be described as a 2D sheet with Cd atoms of the adjacent strings separated by 9.026 Å (Fig. 5).

The use of the bbi ligand in the syntheses gave diverse results. Only the reaction with $[Cd\{SSi(tBuO)_3\}_2]_2$ resulted in the

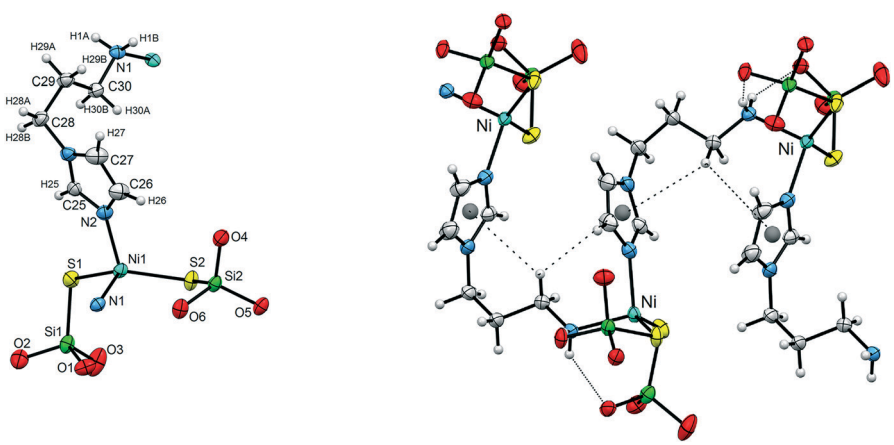

Fig. 3 Left – Molecular structure of **1** with the atom-labeling scheme. Right – The polymeric chain of **1** with weak hydrogen-bonding interactions shown as dashed lines. The *t*Bu groups are omitted for clarity. Thermal ellipsoids are drawn at 30% probability.

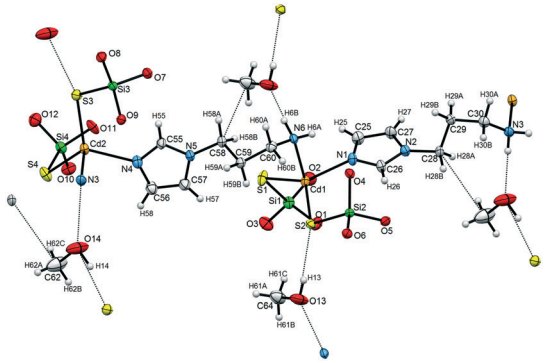

Fig. 4 A view of complex 3 showing all the supramolecular interactions.

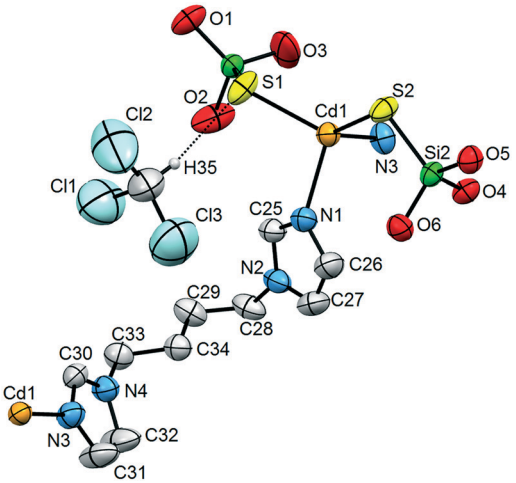

Fig. 6 Molecular structure of 4 with the atom-labeling scheme and the C–H···S hydrogen bonding interaction shown as a dashed line. *t*BuO groups and H atoms not involved in the additional interactions are omitted for clarity.

1D coordination polymer $[Cd\{SSi(tBuO)_3\}_2(\mu\text{-bbi})\cdot 2CHCl_3]_n$ **4**, whereas reaction with $[Co\{SSi(tBuO)_3\}_2(NH_3)]_2$ allowed the obtainment of dimeric $[Co\{SSi(tBuO)_3\}_2(\mu\text{-bbi})_2\cdot 3CH_3OH]_2$ **5**.

As with previous complexes, the metallic centers in both complexes **4** and **5** are also four coordinated resulting in MN_2S_2 kernels. Both Cd and Co atoms adopt a tetrahedral geometry, but the distortions from the ideal geometry are stronger in **4** (τ_4 = 0.85) than in **5** (τ_4 = 0.93). However, they do not affect the M–N and M–S bond lengths and angle values on Cd ions which are comparable with those present in other Cd and Co silanethiolates.[26–28,42]

Compound **4** crystallizes in the $P2_1/c$ space group of the monoclinic system and the asymmetric unit consists of a Cd(II) ion, two terminal $(tBuO)_3SiS^-$, one bbi ligand and one molecule of chloroform (Fig. 6).

The crystal packing of **4** shows that the molecule of solvent forms only one weak C–H···$S_{silanethiolate}$ hydrogen bonding interaction with one S atom of the silanethiolate residue (D···A 3.655 Å). The second S atom is also engaged in the formation of two even weaker C28–H28A···S2 and C34–H34A···S2 interactions with the aliphatic part of the bbi ligand from the neighboring chain of **4** (D···A 3.869 and 3.894 Å, respectively). As a result, the interchain Cd···Cd distances are 11.116 Å and the intrachain distances fall within the range of 9.609–10.011 Å (Fig. 7 and S5 in the ESI†).

Compound **5** crystallizes in the $P\bar{1}$ space group of the triclinic system and the asymmetric unit consists of a Co(II) ion, two terminal $(tBuO)_3SiS^-$, one bbi ligand and three molecules of methanol (Fig. 8). The steric effects of ligands gave rise to a dinuclear structure where cobalt ions are bridged by two bbi ligands *via* the imidazole N atoms, and their coordination sphere is made up of two silanethiolate S atoms. The

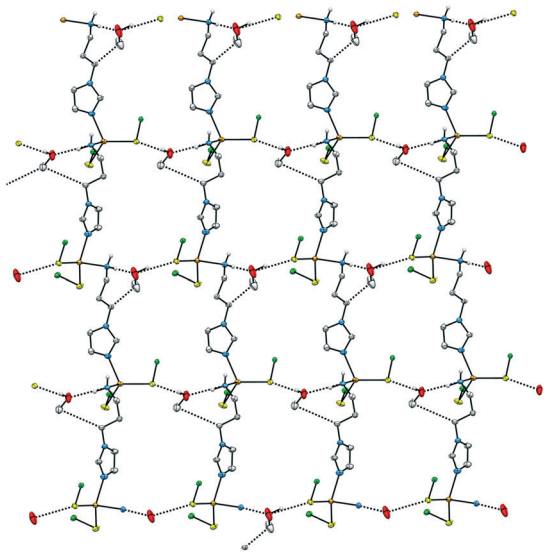

Fig. 5 A view of the 2D structure of compound **3** with hydrogen bonding interactions shown as dashed lines and *t*BuO groups omitted for clarity.

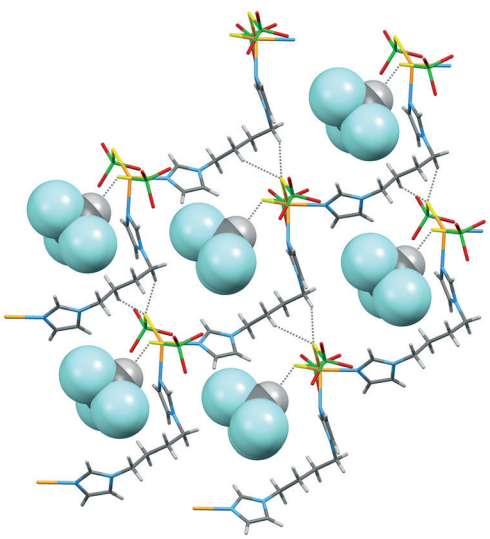

Fig. 7 The crystal packing of **4** with hydrogen bonding interactions shown as dashed lines. *t*BuO groups are omitted for clarity. Atoms of $CHCl_3$ are presented as balls.

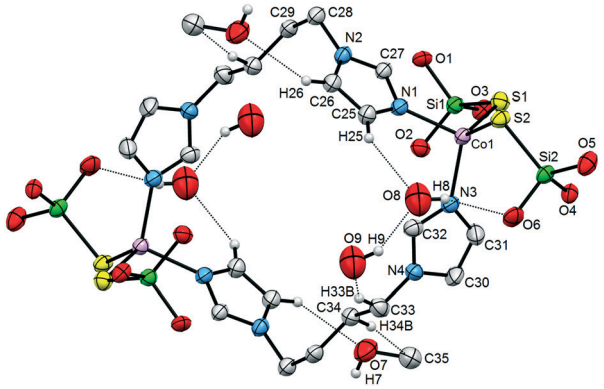

Fig. 8 Molecular structure of **5** with the atom-labeling scheme and hydrogen bonding interactions shown as dashed lines. *t*BuO groups and H atoms not involved in the additional interactions are omitted for clarity.

inversion center, which is placed in the centre of the gap formed by two bbi ligands, generates the second part of the dimer. Further analysis shows that the molecules of methanol form a net of hydrogen bonding interactions. One molecule acts as a double donor of bifurcated O8–H8···O6 and O8–H8···S2 with O and S atoms from the silanethiolate group (D···A distances are 2.845 and 3.599 Å) and as an acceptor of O9–H9···O8 and much weaker C32–H32···O8 interactions with the second molecule of CH_3OH and C–H from the imidazole ring, respectively (D···A distances are 2.679 and 3.344 Å).

The third CH_3OH molecule forms an O7–H7···S1 interaction with the second $(tBuO)_3SiS^-$ residue (D···A distance is 3.245 Å) and additionally is engaged in weak C26–H26···O7 interaction formation with the neighboring dimer of compound **5** (D···A distance is 3.295 Å). Moreover, the extended structure of the compound involves two distinct secondary C–H···π interactions between adjacent dimers which are formed by one imidazole ring from one bbi and a C–H bond from the aliphatic linker of the bbi ligand from the next dimer (D···A distance is 2.808 Å) (Fig. 9 and S6 in the ESI†). Unfortunately, the attempts to obtain a Ni(II) silanethiolate complex with bbi were ultimately not successful. The reaction

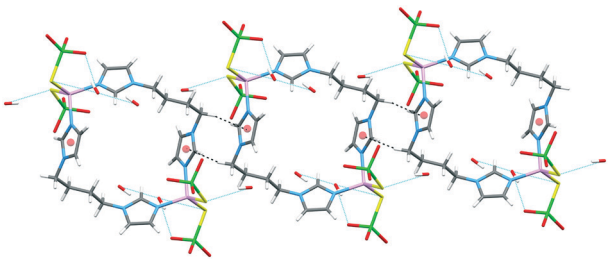

Fig. 9 The arrangement of compound **5** as a chain of dimers connected through a net of hydrogen bonding (shown as blue dashed lines)and C–H···π interactions between adjacent dimers (shown as grey dashed lines). *t*BuO groups and H atoms from methanol molecules are omitted for clarity.

of a nickel ammine complex with $(tBuO)_3SiSH$ and bbi resulted in colorless crystals of tetra-*tert*-butoxy-1,3,2,4-dithiadisiletan $[(tBuO)_3SiS]_2$. This compound was already obtained by *Wojnowski* in the alcoholysis reaction of SiS_2 by *t*-butanol.[43] Nevertheless, we are still trying to find out whether the change of the initial conditions of reaction will allow us to obtain a desirable Ni(II) silanethiolate with bbi.

Up till now the use of a variety of solvents and ratios of the reactants has not resulted in any defined complexes; therefore besides $(tBuO)_3SiSH$ and bbi we choose $Ni(acac)_2 \cdot 2H_2O$ as a primary reagent. This procedure allowed us to obtain small, blue crystals of a new compound $[Ni(acac)_2(\mu\text{-bbi}) \cdot 9CHCl_3]_n$ **6** deprived, however, of silanethiolate ligands (Fig. S7 and S9 in the ESI†). The compound crystallizes in the triclinic space group $P\bar{1}$, and its crystal structure consists of $Ni(acac)_2$ units bridged by a bbi molecule only. Thus, each Ni(II) center is hexacoordinated and is located in an almost regular octahedral environment surrounded by four oxygen atoms from two acac ligands in the equatorial positions and two nitrogen atoms from two bbi molecules in the axial position, resulting in a NiN_2O_4 chromophore. Ni–O bond distances are slightly shorter (range 2.035(4)–2.059(4) Å), and Ni–N are longer (range 2.101(5)–2.127(5) Å) in comparison with the related complexes (Table S2 in the ESI†).[44] The empty spaces between the chains are large enough to accommodate nine molecules of chloroform solvent in the asymmetric unit (Fig. S8 in the ESI†).

They are engaged in the formation of additional interactions with the frameworks, *i.e.* C–H···Cl and Cl···Cl between $CHCl_3$ molecules and $C_{chloroform}$–H···O_{acac} with the chain of **6** and serve also as a connection between adjacent chains. Yet, these molecules are very weakly bonded to the compound, and they leave the crystals immediately after the removal of the crystals from the solution so that the crystals lose their shape and luster.

We have also studied crystalline and homogenous samples of compounds **1**–**5** by powder XRD measurements. Comparison of the obtained powder patterns with the simulated ones derived from the single crystal data with the use of the program Mercury showed major differences (Fig. S10–S15 in the ESI†). Being quite convinced about the structure of crystalline samples confirmed by XRD, EA and microscopy observations, we suppose that the observed discrepancies are due to the decay caused by the milling of the samples before the measurement. All the crystals contain solvent molecules loosely bound in the lattices so powderization (milling) may lead to their weathering.

IR spectroscopy

The IR spectra recorded for all the complexes in the solid state are consistent with their crystal structures. The spectra of complexes **1**–**6** contain strong intensity bands in the range of 3120–2865 cm^{-1} attributed to symmetric and asymmetric C–H stretching modes of the methylene units of ligands api and bbi, and methyl groups from $(tBuO)_3SiS^-$ residues.[45] The

vibrations of the C=C bonds of the imidazole ring can be observed in the range of 1600–1520 cm^{-1} (1528, 1514, 1522, 1498, 1519 and 1509 cm^{-1}, respectively). Another absorption band characteristic of C–N stretching vibrations of the imidazole ring is usually located at about 1090 cm^{-1}. The characteristic bands of the silanethiolato complexes are observed at 1100–980 cm^{-1}, which correspond to the Si–O–C bond of the silanethiolate residue coordinating terminally to the metallic center (Fig. S15 and S16 in the ESI†).[24–30,41,42] The IR spectra of **1**–**3** in the solid state contain several bands in the 3400–3090 cm^{-1} range assigned to the api NH_2 stretching vibrations. The particular frequencies are slightly shifted, which is caused by the presence of diverse hydrogen bond interactions like intramolecular N–H···O in **1** and **2** as well as intermolecular N–H···O and O–H···S interactions in **3**. The spectrum of **5** also contains a broad absorption in the frequency range 3500–3100 cm^{-1} which corresponds to the O–H vibrations of the uncoordinated methanol molecules involved in the hydrogen bonding network in the crystals.

Magnetic properties

The variable-temperature molar magnetic susceptibility ($\chi = M/H$) data for polycrystalline sample **1** measured at the applied dc magnetic field H = 1 kOe are given in Fig. 10 in the form of χT *vs.* T. The high temperature χT value is 1.4 cm^3 K mol^{-1} which is slightly above the value expected for non-interacting Ni(II) S = 1 ions (χT = 1.21 cm^3 K mol^{-1} for g = 2.20). Upon cooling, $\chi T(T)$ initially changes only weakly, but below ~100 K χT increases to reach a maximum value of 1.51 cm^3 K mol^{-1} at ~14 K, and then decreases rapidly attaining a minimum value of 0.6 cm^3 K mol^{-1} at 2 K. The magnetic susceptibility obeys the Curie–Weiss law above 30 K with a Curie constant C = 1.38 cm^3 K mol^{-1} and a positive Weiss constant θ = 1.88 K (Fig. S17 in the ESI†).

Usually, the increase of χT with decreasing temperature is interpreted as the signature of ferromagnetic (FM) coupling between the magnetic centers, whereas the subsequent rapid drop of χT are considered to be the influence of antiferromagnetic (AFM) interactions or/and the effect of zero-field splitting (ZFS). In order to obtain further insight into the magnetic behavior of **1**, extended magnetic measurements have been performed.

The isothermal magnetization curve collected at 2 K is presented in Fig. 10 (inset). We observe a significant divergence from the Brillouin behavior for S = 1 (dot-dashed line in Fig. 10 (inset)). Additionally, the $M(H)$ curve at 2 K is not reversible and shows a coercivity of $H_c \approx 43$ Oe (Fig. 11, inset); a small hysteresis, with $H_c \approx 17$ Oe, is still observed at T = 2.5 K and disappears at T = 3 K (Fig. S19 in the ESI†). It should be noted that the M *vs.* H plots measured at 100, 200 and 300 K show a perfect linear behavior, which discounts the presence of any FM impurity in **1** (see *M(H)* at 300 K in Fig. S18 in the ESI†). Therefore, the hysteresis behavior of $M(H)$ indicates the occurrence in **1** of some kind of long-range ordering of spins at the lowest temperatures.

A further sign of spontaneous magnetization in **1** is provided by χ_{ZFC} and χ_{FC} thermal dependences measured in ZFC and FC regimes under various applied dc magnetic fields (H = 100 Oe, 1 kOe and 5 kOe). $\chi_{ZFC}(T)$ and $\chi_{FC}(T)$ in H = 100 Oe split up at ~8 K (at T < ~2.5 K a small kink was also observed in $\chi_{ZFC}(T)$) (Fig. 11). With the increase of the applied magnetic field, the ZFC–FC splitting temperature decreases and for H = 5 kOe these dependences are superimposed over the whole temperature interval measured (Fig. S20 in the ESI†). The dynamic ac susceptibility measurements of **1** have also been performed. The temperature dependences of the in-phase (χ') and out-of-phase (χ'') susceptibility components reveal a weak frequency dependence of χ' and the appearance of a non-zero χ'' component at T < ~7 K with the maximum near 3 K (Fig. S21 in the ESI†). The values of χ'' are very small compared with the values of χ'. Nevertheless, these results as well as the non-zero coercivity at T < ~3 K and $\chi_{ZFC}(T) - \chi_{FC}(T)$ irreversibility can be related to the appearance in **1** of a weak 2D/3D spontaneous magnetization at very low temperature. **1** consists of one-dimensional polymeric chains in which metal ions are bridged by api (the intra-chain Ni–Ni separation is 7.504 Å). And, in light of the structural data

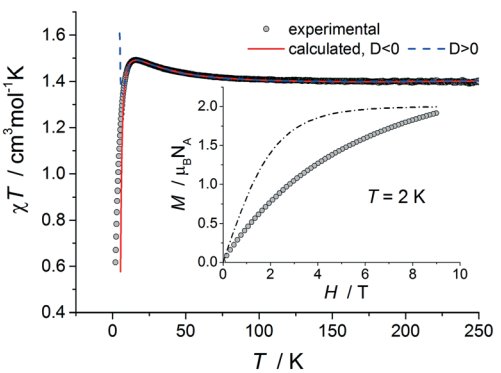

Fig. 10 Plot of χT *versus* T for **1**, measured at 1 kOe (*symbols*) and fitted curves (*solid and dashed lines*). See text for details. Inset: Magnetization curve measured at 2 K for **1** (in μ_B/Ni *vs.* H) (*symbols*) and theoretical Brillouin curve for S = 1 (*dot-dashed line*).

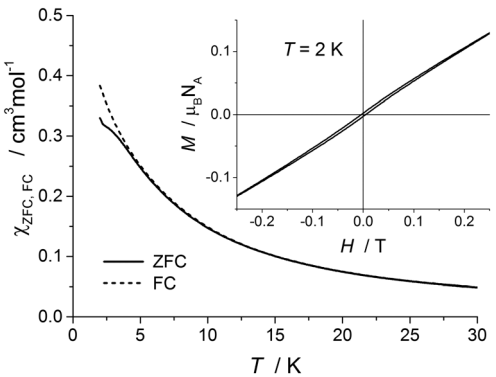

Fig. 11 Temperature dependences of χ_{ZFC} and χ_{FC} magnetic susceptibility measured under an applied field of 100 Oe for **1**. Inset: Hysteresis loop recorded at 2 K for **1**.

reported above, this extended bridging ligand seems to be the main superexchange pathway for the magnetic coupling found in **1** (the shortest inter-chain interaction is ~12.6 Å and there is no binding between the neighbor chains). So, the fit of magnetic data using the model of regular $S = 1$ chains has been performed. Unfortunately, this attempt did not provide a satisfactory result. This can be explained by the significant influence of the single-ion anisotropy of four-coordinated tetrahedral Ni(II) ions (for Ni(II) in tetrahedral geometry the observed D parameters adopt values between −22 and +45 cm^{-1})[46] and for this it is necessary to evaluate the ZFS effect on the chain susceptibility.

Therefore, analysis of the experimental data of **1** was carried out with de Neef's series expansion[47] for a uniform $S = 1$ Heisenberg chain with the contribution of ZFS, as described by the Hamiltonian: $\mathcal{H} = -2J\sum_i \hat{S}_i\hat{S}_{i+1} + D\sum_i(\hat{S}_{iz}^2 - 2/3) + g\mu_B H\sum_i \hat{S}_{iz}$. The same approach was applied recently by Palion-Gazda *et al.*[48] The equations for the magnetic susceptibility for this model were used in the form presented by de Neef (see equations A1–A3 in the ESI†). The temperature-independent van Vleck paramagnetism (χ_{TIP}) has been added to the final expression. In this approach, the experimental data can be very well reproduced in the temperature range from ~12 K to 300 K. However, we have also found that values of the fitting parameters D and J are dependent on the sign of the input value (this can be expected, as there is a correlation between these two parameters in the mathematical expression). So, here we present two sets of the best-fit parameters with $D > 0$ and $D < 0$ (solid and dashed lines in Fig. 10, respectively): (1) $D = 4.87$ cm^{-1}, $J = 1.43$ cm^{-1}, $g = 2.32$, $\chi_{TIP} = 1.4 \times 10^{-4}$ with the agreement factor $R = \sum(\chi - \chi_{calcd})^2/\sum\chi^2 = 1.8 \times 10^{-6}$ and (2) $D = -10.46$ cm^{-1}, $J = -0.43$ cm^{-1}, $g = 2.32$, $\chi_{TIP} = 1.3 \times 10^{-4}$ with $R = 8 \times 10^{-7}$. In both cases, a disagreement of experimental and calculated data appears at $T <$ ~10 K. This can be ascribed to the limited usefulness of de Neef's expressions at very low temperatures (only for $kT > 2J$)[47] and/or the influence of an additional contribution to the magnetic coupling at very low temperatures (as was observed in the magnetic behavior, see above).

In the set of the best-fit parameters (1), a positive J value indicates FM intra-chain coupling. However, $D > 0$ for Ni(II) ions implies a non-magnetic singlet ground state ($M_S = 0$). In such a system, a sufficiently large ZFS contribution (compared to magnetic exchange) prevents the magnetic ordering as $T \to 0$. According to de Neef, this occurs when $D/J > 2$ (for $J > 0$).[47] For D and J values from set (1), the ratio $D/J \approx 3.5$, which gives a noticeable discrepancy between the de Neef prediction and low temperature magnetic results for **1**.

In turn, set (2) gives a negative D value for single Ni(II) ions ($M_S = \pm 1$ ground state) and relatively weak AFM Ni(II)–Ni(II) interactions ($J < 0$). The combination of negative exchange coupling and the observed rise of χT with decreasing temperature (Fig. 10) may indicate the spin-canted structure along the chain, which gives rise to a weak ferromagnetism.[33,49] Such non-collinear spin–spin ordering can result from the relatively large $|D/J|$ ratio (for set (2) $D/J \approx 23.5$) and strongly folded polymeric chain of **1** (see structural information).

Unfortunately, we could not compare the obtained values of J with those of similar complexes consisting 3d ions bounded with a 1-(3-aminopropyl)-imidazole group, as we did not find any references in the literature on that. Furthermore, we should also remember that D and J parameters are correlated, and, therefore, these values might be over or underestimated. Thus, the unequivocal confirmation or exclusion of one of the sets of the best-fit parameters is difficult. Nevertheless, analysis of the experimental data (in the 12–300 K range) reveals the weak intra-chain magnetic interactions which strongly interplay with the single-ion magnetic anisotropy of Ni(II) ions. The magnetic behavior observed at $T < 10$ K is not clear at this stage. For this purpose, as well as for the exact estimation of the D and J parameters, further experimental and theoretical studies are needed.

In Fig. 12(a) the temperature dependence of molar magnetic susceptibility for polycrystalline sample **2** is presented as χT *vs.* T. The χT value at room temperature (2.47 cm^3 K mol^{-1}) is in agreement with the presence of magnetically isolated high-spin Co(II) ions with an orbital contribution to the magnetic moment ($\chi T = 2.48$ cm^3 K mol^{-1} for $g = 2.3$). $\chi T(T)$ smoothly decreases with decreasing temperature in the

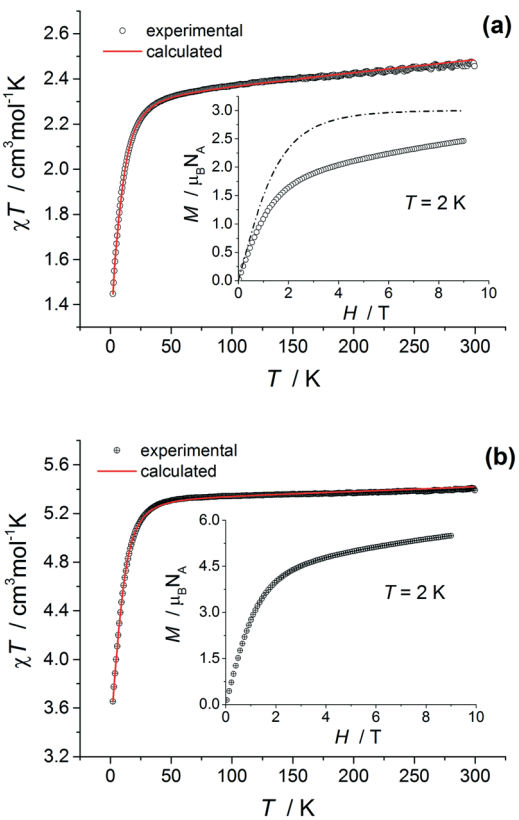

Fig. 12 Experimental (*symbols*) and calculated (*solid line*) values of χT *versus* T (at 1 kOe) for **2** (a) and **5** (b). Insets show the magnetization curves measured at 2 K presented as μ_B/Co *vs.* H for **2** (a) and as μ_B/2Co *vs.* H for **5** (a). The theoretical Brillouin curve for $S = 3/2$ is presented in the inset (a) (*dot-dashed line*).

300–~30 K range, then drops rapidly down to 2 K. The thermal dependence of the reciprocal susceptibility shows linearity (Fig. S17 in the ESI†) and fitting of the χ *vs.* T dependence to the Curie–Weiss law gives the Curie constant C = 2.37 cm^3 K mol^{-1} and Weiss constant θ = −1.47 K ($T > 30$ K). The χ_{ZFC} and χ_{FC} *vs.* T plots measured in H = 1 kOe are superimposed in the whole temperature range measured (Fig. S22 in the ESI†). The magnetization curve at 2 K reveals no hysteresis (Fig. 12(a), inset); the near saturation magnetic moment (measured in 9 T) is 2.46 μ_B per Co ion, which is below the expected value of ~3 μ_B for a Brillouin S = 3/2 model (dot-dashed line in Fig. 12(a), inset).

The high temperature results of magnetic studies of **2** indicate the dominant paramagnetic behavior of cobalt ions. The observed decrease of χT values at low temperatures as well as the reduced near saturation magnetic moment at 2 K can be related to the significant ZFS effect and/or weak AFM interactions. According to the structural information, the Co(II) ions in **2** reside in a distorted tetrahedral geometry. For such a symmetry, Co(II) ions represent a typical ZFS system as the ground term is orbitally nondegenerated $^4A_2$.[50,51] Hence, the experimental $\chi(T)$ dependence of **2** can be analyzed within a spin-Hamiltonian: $\mathcal{H} = g\mu_B\hat{S}\cdot H + D[\hat{S}_z^2 - S(S+1)/3]$, where D is the axial ZFS parameter. In the fitting procedure, the expressions for the susceptibility components χ_z and χ_{xy} of a single-ion system with S = 3/2 reported by Boča[51] have been used (see equations B2 and B3 in the ESI†). The averaged magnetic susceptibility can be expressed as $\chi_{calcd} = (\chi_z + 2\chi_{xy})/3 + \chi_{TIP}$.

For the best fit exchange coupling of the nearest neighbors ($2zJ'$) needs to be taken into consideration (these interactions have been calculated in the usual molecular field approximation[33,50] (equation B4 in the ESI†)). The best set of the fitting parameters is: D = −11.73 cm^{-1}, g_z = 2.27, g_{xy} = 2.20, $2zJ'$ = −0.05 cm^{-1}, $\chi_{TIP} = 5.5 \times 10^{-4}$ and $R = 1.3 \times 10^{-6}$ (solid line in Fig. 12(a)). We are aware that the sign of the D parameter is difficult to determine by a fit of magnetic data for polycrystalline samples. However, the difference between the fits with positive and negative D is significant and for $D > 0$ the fitting agreement is evidently worse. So, here and in the next case we present only the set of parameters that best reproduce the experimental data. The obtained $2zJ'$ value indicates that in **2**, Co(II)–Co(II) magnetic interactions are extremely small and shows the dominant influence of the ZFS effect on the magnetic behavior of this compound.

In Fig. 12(b) the experimental molar susceptibility for the dimeric compound **5** is shown as χT *vs.* T. The high temperature χT value (5.4 cm^3 K mol^{-1}) is close to the expected value for two non-interacting Co(II) ions (χT = 4.96 cm^3 K mol^{-1} for g = 2.3). With decreasing temperature, χT is almost constant until ~50 K, then smoothly decreases and below ~20 K it drops rapidly. $1/\chi(T)$ dependence exhibits linearity and the Curie–Weiss fit gives C = 5.38 cm^3 K mol^{-1} and θ = −0.72 K (Fig. S17 in the ESI†). $\chi_{ZFC}(T)$ and $\chi_{FC}(T)$ dependences measured in H = 1 kOe are superimposed in the 2–300 K range (Fig. S22 in the ESI†). The magnetization curve at 2 K demonstrates zero coercivity and a Brillouin-like shape with a near saturation magnetic moment of 5.5 μ_B per molecule (Fig. 12(b), inset), whereas $M(H)$ at 300 K is perfectly linear (Fig. S18 in the ESI†). The above results indicate the dominant paramagnetic behavior of **5** corresponding to the presence of two magnetically isolated high-spin Co(II) ions per molecule. The cobalt(II) ions in **5** are in a tetrahedral geometry, like in compound **2**, and the experimental χ *vs.* T data of **5** have been analyzed within the spin-Hamiltonian model presented above. The obtained parameters are: D = −11.5 cm^{-1}, g_z = 2.46, g_{xy} = 2.33, $\chi_{TIP} = 4 \times 10^{-4}$ and $R = 3.8 \times 10^{-6}$ (solid line in Fig. 12(b)). It should be noted that the experimental data for **5** can be very well reproduced without taking into account the exchange coupling of the nearest neighbors.

Thus, analysis of the magnetic data of **2** and **5** shows the paramagnetic behavior of cobalt(II) ions which is noticeably influenced by the ZFS effect at low temperatures. The obtained values of the axial ZFS parameter D for these two compounds are very similar, in agreement with the similarity of the coordination environments around the Co(II) centers, and fall within a wide range of values, from +15 cm^{-1} to −161 cm^{-1}, observed for high-spin Co(II) in tetrahedral geometry.[51,52]

Luminescence

Previous studies have shown that coordination compounds of Cd(II) ions may exhibit good luminescence properties.[53] Therefore, we decided to investigate the luminescence properties of the newly obtained complexes of Cd(II) ions **3** and **4**. The emission spectra of the Cd complexes were recorded in the solid state at ambient temperature and are depicted in Fig. 13 and 14. The main chromosphere of the studied compounds is the aromatic five-membered imidazole ring. The main emission peaks of the free ligands api and bbi appear at 417.6 and 440.8 nm (λ_{ex} = 377 nm) for api and at 393.2 nm (λ_{ex} = 336 nm) for bbi. The emission bands of these free ligands are probably attributable to the π*–π or π*–n transitions.[54] As shown in Fig. 13, the emission bands of

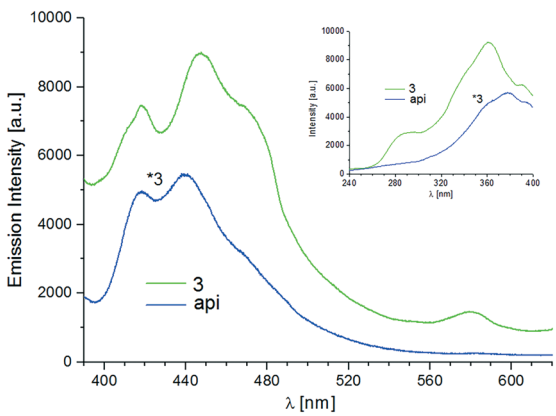

Fig. 13 The emission spectra of ligand api and complex **3**; the insert presents the excitation spectra of api and **3**.

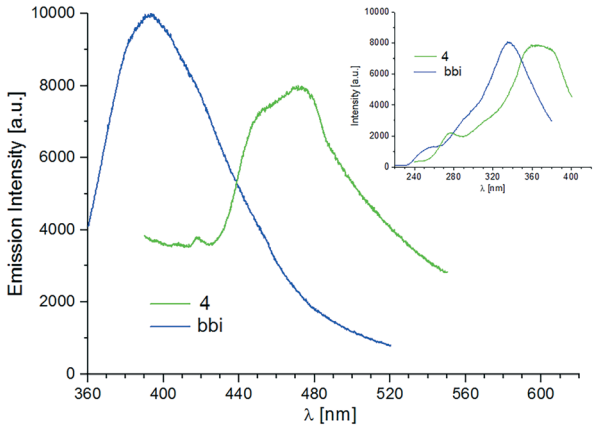

Fig. 14 The emission spectra of ligand bbi and complex **4**; the insert presents the excitation spectra of bbi and **4**.

compound **3** are observed at 418.4 and 447.8 nm (λ_{ex} = 362 nm). The positions of the emission peaks are similar to those of the ligand api. Hence, these emission peaks can be ascribed to intraligand transitions modified by metal coordination.[55] The luminescence intensity of solid **3** is stronger than that of the liquid api.

The enhancement of luminescence in compound **3** may be attributed to the coordination effect of the ligand to Cd(II) ions, which effectively increases the rigidity of the ligand and reduces the loss of energy by radiationless decay.[56] Under the same experimental conditions, compound **4** produces an emission spectrum with a maximum at 471.4 nm (λ_{ex} = 362 nm, Fig. 14). Compared to the ligand bbi, a significant red shift (78 nm) for this compound has been observed. The emission of **4** may be assigned to ligand to metal charge transfer (MLCT).[57] Besides this, weak emission bands located at about 579 nm in both compounds are also due to MLCT.

TG analysis

Thermal analysis (TG) was applied to investigate the thermal stability and behavior of complexes **1**–**5**. The results are shown in Fig. S23 in the ESI.† The thermal decomposition patterns of complexes **1**–**3** are comparable – they are stable at room temperature, whereas further heating leads to melting and degradation processes resulting in metal sulfides (for **1** calc. wt% = 12.22, found wt% = 12.54, **2** calc. wt% = 14.78, found wt% = 12.29, **3** calc. wt% =8.81, found wt% = 7.01, **4** calc. wt% = 14.72, found wt% = 16.02, **5** calc. wt% = 10.06, found wt% = 10.58).

Compounds **1** and **2** decompose in a one-step process at about 209 °C and 232–247 °C, respectively, whereas complex **3** decomposes in a two-stage process in the range 170–256 °C. The first weight loss step in **3** is observed at about 170 °C, which corresponds to the loss of solvent molecules. In the second weight loss step, complex **3** decomposes gradually in the temperature range of 237–256 °C with the loss of $(t\text{BuO})_3\text{SiS}^-$ residues and the bridging N-donor ligands. The curves of thermal decomposition of compounds **4** and **5** exhibit three or four pronounced weight loss steps. The decomposition of **4** starts at about 101 °C and corresponds to the loss of a chloroform molecule (calc. 12.18%, found 11,85%). The next degradation steps occur within the range 180–324 °C. Compound **5** starts to decompose at about 255 °C with almost 42% of weight loss and further decomposes progressively up to about 525 °C.

The progress of decomposition was also monitored with the FTIR spectrum of the selected complex **5** and our choice relies on the fact that obtained silanethiolates are based on the same types of ligands. The spectrum of the decomposition of compound **5** is similar to those described previously[26] and shows the presence of gaseous products of the decomposition of tri-*tert*-butoxysilyl substituents containing both Si–OH ($\nu_{(Si-O)}$ = 1074 cm^{-1}) and Si–O–*t*Bu ($\nu_{(C-O)}$ = 1193 cm^{-1}) fragments (Fig. S24 in the ESI†). The spectrum also exhibits additional bands observed for symmetric and asymmetric scissor-bending vibrations characteristic of *tert*-butyl residues (1394, 1371, 1243 and 1193 cm^{-1}) as well as of CH_2 groups present in aliphatic carbon chains of N-donor ligands (1477 cm^{-1}).

Conclusions

In summary, we showed that the introduction of api and bbi to different building units allows the synthesis of new Co(II), Cd(II) and Ni(II) compounds with diverse structure and topology. It was found that the presence of additional hydrogen bonding interactions in **3** results in the formation of a 2D framework built from polymeric chains combined by a net of H-bonding interactions and solvent molecules as bridges. In addition, the luminescence properties of **3** and **4** cadmium complexes were studied in the solid state at room temperature. The emissions were ascribed to intraligand transitions in **3** and ligand to metal charge transfer in **4**. Magnetic investigations of **1** reveal the presence of weak intra-chain magnetic coupling between nickel(II) ions. Analysis of the variable-temperature magnetic susceptibility data using a model for a uniform S = 1 Heisenberg chain in combination with the zero-field splitting effect suggests the interplay of the magnetic interactions with the single-ion magnetic anisotropy of Ni(II) ions. In turn, compounds **2** and **5** show paramagnetic behavior. The experimental $\chi(T)$ dependences for these compounds have been analyzed on the basis of a spin-Hamiltonian for a mononuclear S = 3/2 system with the addition of zero-field splitting.

Our further studies are directed towards the synthesis of higher dimensional networks based on silanethiolate derivatives and N-donor organic linkers as well as the investigation of their magnetic and photoactive properties.

Acknowledgements

The studies were supported by Polish National Science Centre grant no. 2013/09/B/ST5/03479. Magnetic measurements were performed in the laboratory of NanoFun, POIG.02.02.00-00-

025/09. The authors also thank the anonymous reviewers who generously shared their knowledge with us.

References

1 J. M. Berg, J. L. Tymoczko, G. J. Gatto and L. Stryer, *Biochemistry*, W. H. Freeman & Company, New York, 2015.
2 Y. Li and D. B. Zamble, *Chem. Rev.*, 2009, **109**, 4617–4643.
3 M. Can, F. A. Armstrong and S. W. Ragsdale, *Chem. Rev.*, 2014, **114**, 4149–4174.
4 R. B. Silverman and M. W. Holladay, *The Organic Chemistry of Drug Design and Drug Action*, Academic Press, San Diego, 2014.
5 T. Nakamura, H. Kakinuma, H. Umemiya, H. Amada, N. Miyata, K. Taniguchi, K. Bando and M. Sato, *Bioorg. Med. Chem. Lett.*, 2004, **14**, 333–336.
6 H. Katsumi, M. Nishikawa, R. Hirosaki, T. Okuda, S. Kawakami, F. Yamashita, M. Hashida, T. Sakane and A. Yamamoto, *Mol. Pharmaceutics*, 2016, **13**, 2867–2873.
7 F.-M. Klingler, T. A. Wichelhaus, D. Frank, J. Cuesta-Bernal, J. El-Delik, H. F. Müller, H. Sjuts, S. Göttig, A. Koenigs, K. M. Pos, D. Pogoryelov and E. Proschak, *J. Med. Chem.*, 2015, **58**, 3626–3630.
8 C. F. Shaw, *Chem. Rev.*, 1999, **99**, 2589–2600.
9 R. A. Santos, E.-S. Gruff, S. A. Koch and G. S. Harbison, *J. Am. Chem. Soc.*, 1990, **112**, 9257–9263.
10 C. A. Grapperhaus and M. Y. Darensbourg, *Acc. Chem. Res.*, 1998, **32**, 451–459.
11 L. Lermer, Y. Roupioz, R. Ting and D. M. Perrin, *J. Am. Chem. Soc.*, 2004, **124**, 9960–9961.
12 S. Groysman and R. H. Holm, *Biochemistry*, 2009, **48**, 2310–2320.
13 M. Gennari, M. Orio, J. Pecaut, F. Neese, M.-N. Collomb and C. Duboc, *Inorg. Chem.*, 2010, **49**, 6399–6401.
14 S. Kaur-Ghumaan and M. Stein, *Dalton Trans.*, 2014, **43**, 9392–9405.
15 J. Liu, L. Chen, H. Cui, J. Zhang, L. Zhang and C.-Y. Sum, *Chem. Soc. Rev.*, 2014, **43**, 6011–6061.
16 E. P. Broering, S. Dillon, E. M. Gale, R. A. Steiner, J. Telser, T. C. Brunold and T. C. Harrop, *Inorg. Chem.*, 2015, **54**, 3815–3828.
17 I. Nath, J. Chakraborty and F. Verpoort, *Chem. Soc. Rev.*, 2016, **45**, 4127–4170.
18 M. A. Halcrow and G. Christou, *Chem. Rev.*, 1994, **94**, 2421–2481.
19 J. A. Denny and M. Y. Darensbourg, *Chem. Rev.*, 2015, **115**, 5248–5273.
20 R. Pulukkody and M. Y. Darensbourg, *Acc. Chem. Res.*, 2015, **48**, 2049–2058.
21 B. Żurowska, J. Mroziński, M. Julve, F. Lloret, A. Maslejova and W. Sawka-Dobrowolska, *Inorg. Chem.*, 2002, **41**, 1771–1777.
22 D. T. Corwin Jr., E. S. Gruff and S. A. Koch, *J. Chem. Soc., Chem. Commun.*, 1987, 966–967; D. T. Corwin Jr. and S. A. Koch, *Inorg. Chem.*, 1988, **27**, 493–496.
23 R. Piękoś and W. Wojnowski, *Z. Anorg. Allg. Chem.*, 1962, **318**, 212–216; A. Herman, B. Becker and W. Wojnowski, *Z. Anorg. Allg. Chem.*, 1979, **450**, 178–182.
24 A. Dołęga, W. Marynowski, K. Baranowska, M. Śmiechowski and J. Stangret, *Inorg. Chem.*, 2012, **51**, 836–843; A. Dołęga, A. Jabłońska, A. Pladzyk, Ł. Ponikiewski, W. Ferenc, J. Sarzyński and A. Herman, *Dalton Trans.*, 2014, **43**, 12766–12775.
25 A. Mielcarek, M. Daszkiewicz, K. Kazimierczuk, A. Ciborska and A. Dołęga, *Acta Crystallogr., Sect. B: Struct. Sci., Cryst. Eng. Mater.*, 2016, **72**, 763–770; A. Ciborska, E. Conterosito, M. Milanesio, K. Kazimierczuk, K. Rzymowska, K. Brzozowski and A. Dołęga, *Eur. J. Inorg. Chem.*, 2015, **19**, 3059–3065; S. Godlewska, K. Baranowska and A. Dołęga, *Inorg. Chem. Commun.*, 2014, **40**, 69–72; S. Godlewska, J. Jezierska, K. Baranowska, E. Augustin and A. Dołęga, *Polyhedron*, 2013, **65**, 288–297; K. Baranowska, N. Piwowarska, A. Herman and A. Dołęga, *New J. Chem.*, 2012, **36**, 1574–1582; A. Pladzyk, Ł. Ponikiewski, Y. Lan and A. K. Powell, *Inorg. Chem. Commun.*, 2012, **20**, 66–69; A. Kropidłowska, J. Chojnacki and B. Becker, *Inorg. Chem. Commun.*, 2006, **9**, 383–387; A. Dołęga, A. Konitz, E. Baum and W. Wojnowski, *Acta Crystallogr., Sect. B: Struct. Sci., Cryst. Eng. Mater.*, 2005, **61**, m2582–m2584; K. Peters, E.-M. Peters, H. G. Von Schnering, W. Wojnowski and S. Tamulewicz, *Z. Kristallogr. - New Cryst. Struct.*, 1998, **13**, 347–348; B. Becker, K. Radacki and W. Wojnowski, *J. Organomet. Chem.*, 1996, **521**, 39–49; B. Becker, W. Wojnowski, K. Peters, E.-M. Peters and H. G. Von Schnering, *Inorg. Chim. Acta*, 1993, **214**, 9–11; B. Becker, W. Wojnowski, K. Peters, E.-M. Peters and H. G. Von Schnering, *Polyhedron*, 1992, **11**, 613–616.
26 A. Pladzyk and K. Baranowska, *J. Mol. Struct.*, 2014, **1058**, 252–258; A. Pladzyk, K. Baranowska, K. Dziubińska and Ł. Ponikiewski, *Polyhedron*, 2013, **50**, 121–130.
27 A. Pladzyk, Ł. Ponikiewski, A. Dołęga, K. Słowy, A. Sokołowska, K. Dziubińska and Z. Hnatejko, *Chem. – Asian J.*, 2015, **10**, 2388–2396; A. Pladzyk, Z. Hnatejko and K. Baranowska, *Polyhedron*, 2014, **79**, 116–123; A. Pladzyk, Ł. Ponikiewski, N. Stanulewicz and Z. Hnatejko, *Opt. Mater.*, 2013, **36**, 554–561; A. Pladzyk, K. Baranowska, D. Gudat, S. Godlewska, M. Wieczerzak, J. Chojnacki, M. Bulman, K. Januszewicz and A. Dołęga, *Polyhedron*, 2011, **30**, 1191–1200; A. Dołęga and M. Walewski, *Magn. Reson. Chem.*, 2007, **45**, 410–415.
28 P. Maślewski, K. Kazimierczuk, Z. Hnatejko and A. Dołęga, *Inorg. Chim. Acta*, 2017, **459**, 22–28; A. Dołęga, K. Baranowska, D. Gudat, A. Herman, J. Stangret, A. Konitz, M. Śmiechowski and S. Godlewska, *Eur. J. Inorg. Chem.*, 2009, 3644–3660; A. Dołęga, A. Pladzyk, K. Baranowska and J. Jezierska, *Inorg. Chim. Acta*, 2009, **362**, 5085–5096; A. Dołęga, A. Farmas, K. Baranowska and A. Herman, *Inorg. Chem. Commun.*, 2009, **12**, 823–827; A. Dołęga, K. Baranowska, A. Pladzyk and K. Majcher, *Acta Crystallogr., Sect. C: Struct. Chem.*, 2008, **64**, m259–m263.
29 B. Becker, A. Zalewska, A. Konitz and W. Wojnowski, *Z. Anorg. Allg. Chem.*, 2001, **627**, 271–279.
30 W. Wojnowski, B. Becker, L. Walz, K. Peters, E.-M. Peters and H. G. Von Schnering, *Polyhedron*, 1992, **11**, 607–612.
31 J. Yang, J. F. Ma, Y. Y. Liu, S. L. Li and G. L. Zheng, *Eur. J. Inorg. Chem.*, 2005, 2174–2180; J. Z. Vlahakis, S. Mitu, G.

Roman, E. P. Rodriguez, I. E. Crandall and W. A. Szarek, *Bioorg. Med. Chem.*, 2011, **19**, 6525–6542.
32 G. A. Bain and J. F. Berry, *J. Chem. Educ.*, 2008, **85**, 532–536.
33 O. Kahn, *Molecular Magnetism*, VCH Publishers, Inc., 1993.
34 STOE and C. GmbH, X-area 2015: Darmstadt. p. software package for collecting single-crystal data on STOE area-detector diffractometers, for image processing, scaling reflection intensities and for outlier rejection.
35 *CrysAlisPro version 1.171*, Oxford Diffraction, Yarnton, England, 2009.
36 G. M. Sheldrick, *Acta Crystallogr., Sect. C: Struct. Chem.*, 2008, **64**, 112–122.
37 L. J. Farrugia, *J. Appl. Crystallogr.*, 1999, **32**, 837–838.
38 O. V. Dolomanov, L. J. Bourhis, R. J. Gildea, J. A. K. Howard and H. Puschmann, *J. Appl. Crystallogr.*, 2009, **42**, 339–341.
39 A. L. Spek, *Acta Crystallogr., Sect. C: Cryst. Struct. Commun.*, 2015, **71**, 9–18.
40 A. W. Addison, T. N. Rao, J. Reedijk, J. van Rijn and G. C. Verschoor, *J. Chem. Soc., Dalton Trans.*, 1984, 1349–1356; L. Yang, D. R. Powell and R. P. Houser, *Dalton Trans.*, 2007, 955–964.
41 Ł. Ponikiewski, A. Pladzyk, W. Wojnowski and B. Becker, *Polyhedron*, 2011, **30**, 2400–2405; A. Pladzyk, A. Ozarowski and Ł. Ponikiewski, *Inorg. Chim. Acta*, 2016, **440**, 84–93.
42 B. Becker, A. Zalewska, A. Konitz and W. Wojnowski, *Polyhedron*, 2001, **20**, 2567–2576; B. Becker, A. Zalewska, A. Konitz and W. Wojnowski, *Appl. Organomet. Chem.*, 2002, **16**, 517–524; A. Pladzyk, J. Olszewska, K. Baranowska and A. M. Dziurzyńska, *Transition Met. Chem.*, 2010, **35**, 821–827; A. Pladzyk, K. Baranowska and P. Hapter, *Transition Met. Chem.*, 2010, **35**, 373–379; A. Pladzyk and K. Baranowska, *Acta Crystallogr., Sect. E: Struct. Rep. Online*, 2007, **63**, m1594; A. Pladzyk and K. Baranowska, *Acta Crystallogr., Sect. E: Struct. Rep. Online*, 2006, **62**, m2602–m2604.
43 W. Wojnowski, K. Peters, D. Weber and H. G. Von Schnering, *Z. Anorg. Allg. Chem.*, 1984, **519**, 134–140.
44 Y. Qi, F. Luo, Y. Che and J. Zheng, *Cryst. Growth Des.*, 2008, **8**, 606–611; X. Duan, Y. Li, F. Wang, C. Lu, Q. Meng and Q. Zhang, *Inorg. Chem. Commun.*, 2010, **13**, 1239–1243; L.-H. Zhang, Y.-Y. Liu, J.-F. Ma, J. Yang, L.-G. Zhang, J. Li and Y.-W. Li, *Polyhedron*, 2011, **30**, 764–777; H. Chen, D. Xiao, J. He, Z. Li, G. Zhang, D. Sun, R. Yuan, E. Wang and Q.-L. Luo, *CrystEngComm*, 2011, **13**, 4988–5000; Y. Zhao and K.-Q. Wang, *Z. Kristallogr. - New Cryst. Struct.*, 2013, **228**, 363–364.
45 K. Nakamoto, *Infrared and Raman Spectra of Inorganic and Coordination Compounds*, John Wiley & Sons, Inc, 5th edn, 1997.
46 P. J. Desrochers, J. Telser, S. A. Zvyagin, A. Ozarowski, J. Krzystek and D. A. Vicic, *Inorg. Chem.*, 2006, **45**, 8930–8941; S. D. Jiang, D. Maganas, N. Levesanos, E. Ferentinos, S. Haas, K. Thirunavukkuarasu, J. Krzystek, M. Dressel, L. Bogani, F. Neese and P. Kyritsis, *J. Am. Chem. Soc.*, 2015, **137**, 12923–12928.
47 T. de Neef, Some applications of series expansions in magnetism, *Ph.D. Thesis*, Technische Hogeschool Eindhoven, Eindhoven, 1975.
48 J. Palion-Gazda, B. Machura, F. Lloret and M. Julve, *Cryst. Growth Des.*, 2015, **15**, 2380–2388.
49 D. F. Weng, Z. M. Wang and S. Gao, *Chem. Soc. Rev.*, 2011, **40**, 3157–3181 and references therein.
50 R. L. Carlin, *Magnetochemistry*, Springer-Verlag, 1986.
51 R. Boča, *Coord. Chem. Rev.*, 2004, **248**, 757–815.
52 M. R. Saber and K. R. Dunbar, *Chem. Commun.*, 2014, **50**, 12266; S. Gómez-Coca, D. Aravena, R. Morales and E. Ruiz, *Coord. Chem. Rev.*, 2015, **289–290**, 379–392; A. K. Bar, C. Pichon and J. P. Sutter, *Coord. Chem. Rev.*, 2016, **308**, 346–380.
53 S.-M. Fang, Q. Zhang, M. Hu, X.-G. Yang, L.-M. Zhou, M. Du and C.-S. Liu, *Cryst. Growth Des.*, 2010, **10**, 4773–4785; N. Zhao, W. Li, C. Sun, Y. Bian, H. Wang, Z. Chang and H. Fan, *Solid State Sci.*, 2012, **14**, 317–323; S.-Z. Ge, Q. Liu, S. Deng, Y.-Q. Sun and Y.-P. Chen, *J. Inorg. Organomet. Polym.*, 2013, **23**, 571–578; H.-Y. Liu, J.-F. Ma, Y.-Y. Liu and J. Yang, *CrystEngComm*, 2013, **15**, 2699–2708.
54 X. Zhang, Y.-Q. Zhao, Z.-C. Hao and G. H. Cui, *J. Inorg. Organomet. Polym.*, 2016, **26**, 1014–1022; H.-H. Wang, H.-Y. Yang, C.-H. Shu, Z.-Y. Chen, L. Hou and Y.-Y. Wang, *Cryst. Growth Des.*, 2016, **16**, 5394–5402.
55 Y.-H. Yu, H.-T. Ye, G.-F. Hou, C.-Y. Ren, J.-S. Gao and P.-F. Yan, *Cryst. Growth Des.*, 2016, **16**, 5669–5677; L. Shen, Y. Bai, Y.-T. Min, T.-T. Jia, Q. Wu, J. Wang, F. Geng, H.-J. Cheng, D.-R. Zhu, J. Yang and G.-W. Yang, *J. Solid State Chem.*, 2016, **244**, 129–139; S.-J. Zhan, Y. Sun, S.-P. Li, G.-M. Tang, Y.-T. Wang and Y.-Z. Cui, *Polyhedron*, 2017, **121**, 252–263; X.-M. Meng, X. Zhang, P.-F. Qi, Z.-A. Zong, F. Jin and Y.-H. Fan, *RSC Adv.*, 2017, **7**, 4855–4871.
56 X. Zhang, X.-Q. Wang, X.-X. Wang, Z.-J. Xue and T.-P. Hu, *Inorg. Chem. Commun.*, 2016, **73**, 21–25; Z. Xu, X. Mao, P. Zhang, H. Li, Y. Wang, M. Liu and L. Jia, *J. Mol. Struct.*, 2017, **1128**, 665–673; F. A. Mautner, C. Berger, R. C. Fischer and S. S. Massoud, *Polyhedron*, 2016, **111**, 86–93.
57 A. Di Santo, G. A. Echeverría, O. E. Piro, H. Perez, A. B. Altabef and D. M. Gil, *J. Mol. Struct.*, 2017, **1134**, 492–503; S.-Y. Mo, D.-L. Fang, B.-Y. Yu and S.-H. Tang, *Polyhedron*, 2017, **123**, 90–98; S.-H. Zhang, J.-M. Wang, H.-Y. Zhang, Y.-P. Fan and Y. Xiao, *Dalton Trans.*, 2017, **46**, 410–419.